IEEE Access
Multidisciplinary | Rapid Review | Open Access Journal

Received December 30, 2019, accepted February 21, 2020, date of publication April 1, 2020, date of current version April 10, 2020.

Digital Object Identifier 10.1109/ACCESS.2020.2983316

Hyperbolic Tangent Function-Based Finite-Time Sliding Mode Control for Spacecraft Rendezvous Maneuver Without Chattering

ZHEN SHI[1], CHENGCHEN DENG[1], SAI ZHANG[2], YAEN XIE[1], HONGTAO CUI[2], AND YONG HAO[1]

[1]College of Automation, Harbin Engineering University, Harbin 150001, China
[2]College of Aerospace and Civil Engineering, Harbin Engineering University, Harbin 150001, China

Corresponding author: Zhen Shi (shizhen@hrbeu.edu.cn)

This work was supported in part by the Major Program of National Natural Science Foundation of China under Grant 61690214, in part by the Natural Science Foundation of Heilongjiang Province under Grant F2017005, in part by the Project under Grant D020214, and in part by the National Key Research and Development Program of China under Grant 2016YFB0501003.

ABSTRACT This paper investigates the robust finite-time rendezvous maneuver control for spacecraft via sliding mode control technology. Two control architectures are devised for realizing the control objective, where a novel-developed sliding mode surface (SMS) is designed by resorting to the hyperbolic tangent function. Without considering the chattering problem inherent in sliding mode control, a basis control scheme is constructed to force the tracking errors entering a compact set in finite time. To reduce the effect of the chattering phenomenon, a modified controller is established by resorting to the well-designed adaptive laws. Both of these two controllers can ensure finite-time convergence for the entire system. Theoretical analysis and numerical simulations have shown the effectiveness and superiorities of the proposed methods.

INDEX TERMS Spacecraft rendezvous maneuver, finite-time control, sliding mode control, chattering problem, adaptive control.

I. INTRODUCTION

For the indispensable role in numerous space activities, including docking, removing space debris, Mars exploration, etc., spacecraft rendezvous maneuver control has gained popularity during the last decades. However, the complexity of the external environment and strongly coupled nonlinear dynamics make it a tough work to design controllers for rendezvous maneuver. Besides, controllers with high precision and satisfactory disturbance rejection performance become more and more desirable for different space missions, which is an urgent issue for aerospace applications. Fortunately, fruitful research achievement for spacecraft control has emerged recently, such as adaptive control [1]–[4], [32], backstepping control [5]–[8], neural network-based control [9]–[12], sliding mode control (SMC) [13]–[16], model predictive control [31] as well as control based on hybrid actuators [35].

The associate editor coordinating the review of this manuscript and approving it for publication was Fangfei Li.

Though effective, the aforementioned methods cannot be directly utilized for spacecraft rendezvous maneuver. During the controller synthesis process in rendezvous missions, the external disturbance, system parameter uncertainties and coupled nonlinear dynamics must be carefully treated, otherwise degradation of control performance or unstable phenomenon will occur in space missions. To handle the disturbance, backstepping based controllers have been established in [17]–[19], where the parameter uncertainties are neglected. Considering that the mass and initial matrix of the pursuer spacecraft are unknown for designers, Zhang et.al have proposed output feedback controllers for relative pose control problem during rendezvous maneuver [20]. It is noticeable that rendezvous maneuver control with collision avoidance is not considered in [17]–[20], probably leading to unexpected casualty. Actually, when the pursuer spacecraft is moving towards the target spacecraft, they may collide with each other. Moreover, there always exist variety of obstacles in space environment, such as space debris, which will threaten the safety of the pursuer spacecraft. In order to endow the control systems with collision avoidance ability,

This work is licensed under a Creative Commons Attribution 4.0 License. For more information, see https://creativecommons.org/licenses/by/4.0/

artificial potential function-based SMC and backstepping control has been presented in [21] and [22], respectively. Recalling the results in [20]–[22], it is obviously that actuator faults and input saturation constraints are not considered, which will limit the application of these researches. By utilizing the anti-saturation controllers designed in [19], rendezvous and docking maneuver can be realized with acceptable performance for rigid spacecraft. In view of the reliability of spacecraft system in rendezvous tasks, fault-tolerant controllers are constructed in [23].

Obviously, results mentioned above can only achieve asymptotic stability for the spacecraft rendezvous maneuver. In contrast to these asymptotically stable methods, finite-time control methods have much more superior qualities in convergence rate, robustness against disturbance and control accuracy [14]–[16], and leading to wide applications in spacecraft rendezvous maneuver [24]–[27]. In [24], nonsingular terminal sliding mode control technology (NTSMCT) was utilized to solve the control issue for spacecraft rendezvous maneuver by incorporation with a finite-time disturbance observer. Totally different from the method proposed in [24], a finite-time algorithm was presented in [25] by resorting to the line-of-sight based control strategy. For the purpose of improving the system robustness against the input saturation constraints, adaptive laws and NTSMCT has been exploited for the anti-saturation issue of rendezvous maneuver [26]. As a technology extension of [26], a novel SMC method was given in [27], which could ensure the accomplishment of rendezvous maneuver without violation of the safe constraints.

Among these existing methods, SMC possesses good ability for disturbance rejection, especially when there exists disturbances and system uncertainties simultaneously. Nevertheless, controllers in [24] suffers severely from the chattering problem, which is the main cause for actuator damage. Thus, it still needs efforts to improve this disadvantage in controller design for aerospace engineering. In this paper, the finite-time rendezvous control for spacecraft will be investigated with the consideration of chattering problem in sliding mode control. Contributions of this paper are given as follows:

i) A novel SMS will be designed by resorting the hyperbolic tangent function. In contrast to literatures [15], [16], the presented SMS is not only nonsingular but also concise and intuitionistic. Specifically speaking, a nonlinear piecewise function was applied for singularity avoidance purpose, which gives rise to much complexity in implementation. By the utilization of the hyperbolic tangent function, this problem will be solved in this paper.

ii) The presented algorithm in this paper can reduce chattering even the sliding mode method is adopted. With the aid of a nonlinear term, the sign function in the control law is replaced, thus avoiding the adverse effect in chattering.

iii) Compared with the results in [18]–[22], global finite-time convergence will be derived for the entire system, effectively improve the convergence rate for spacecraft rendezvous maneuver.

The remainder of this paper is presented as follows. The preliminaries and problem formulation are given. The rendezvous maneuver controller is developed in section III. Numerical simulations are conducted to illustrate the effectiveness of the proposed method. Finally, it comes to the conclusions of this paper.

II. ATTITUDE DYNAMICS AND PROBLEM FORMULATION

A. RELATIVE ATTITUDE DYNAMIC MODEL

In this paper, the relative attitude dynamic will be established via the unit quaternion. Firstly, we define $\boldsymbol{R} \in SO(3)$ as the rotation matrix, which can realize the coordinate transformation. The unit quaternion is described as $\boldsymbol{Q} = \left[q_0, \boldsymbol{q}_v^{\mathrm{T}}\right]^{\mathrm{T}} \in \Xi$ with $\Xi = \left\{\boldsymbol{Q} \in \mathbb{R} \times \mathbb{R}^{3\times 3} \,\middle|\, q_0^2 + \boldsymbol{q}_v^{\mathrm{T}}\boldsymbol{q}_v = 1\right\}$. If the attitude of the pursuer and the target spacecraft are denoted as $\boldsymbol{Q}_p$ and $\boldsymbol{Q}_t$, respectively, the relative attitude between $\boldsymbol{Q}_p$ and $\boldsymbol{Q}_t$ can be expressed as $\tilde{\boldsymbol{Q}} = \left[\tilde{q}_0, \tilde{\boldsymbol{q}}_v^{\mathrm{T}}\right]^{\mathrm{T}} = \boldsymbol{Q}_t^{-1} \odot \boldsymbol{Q}_p$ with $\odot$ denoting the unit quaternion product. Then, the relative attitude kinematics model is given as [28]:

$$\dot{\tilde{q}}_0 = -\frac{1}{2}\tilde{\boldsymbol{q}}_v^T \tilde{\boldsymbol{\omega}} \tag{1}$$

$$\dot{\tilde{\boldsymbol{q}}}_v = \frac{1}{2}\left(\tilde{\boldsymbol{q}}_v^{\times} + \tilde{q}_0 \boldsymbol{I}_3\right)\tilde{\boldsymbol{\omega}} \tag{2}$$

where $\tilde{\boldsymbol{\omega}} = \boldsymbol{\omega}_p - \tilde{\boldsymbol{R}}\boldsymbol{\omega}_t$ is relative angular velocity; $\boldsymbol{\omega}_p$ is the angular velocity of the pursuer; $\boldsymbol{\omega_t}$ is the angular velocity of the target. For a vector $\boldsymbol{a} = [a_1, a_2, a_3]^{\mathrm{T}}$, $\boldsymbol{a}^{\times}$ is defined as Eq. (3). The rotation matrix is defined as Eq. (4).

$$\boldsymbol{a}^{\times} = \begin{bmatrix} 0 & -a_3 & a_2 \\ a_3 & 0 & -a_1 \\ -a_2 & a_1 & 0 \end{bmatrix} \tag{3}$$

$$\tilde{\boldsymbol{R}} \triangleq \boldsymbol{R}\left(\tilde{\boldsymbol{q}}\right) = \left(\tilde{q}_0^2 - \tilde{\boldsymbol{q}}_v^T \tilde{\boldsymbol{q}}_v\right)\boldsymbol{I}_3 + 2\tilde{\boldsymbol{q}}_v\tilde{\boldsymbol{q}}_v^T - 2\tilde{q}_0\tilde{\boldsymbol{q}}_v^{\times} \tag{4}$$

Based on the above expression, the corresponding attitude dynamics of pursuer and the target spacecraft are shown as:

$$\boldsymbol{J}_t\dot{\boldsymbol{\omega}}_t + \boldsymbol{\omega}_t^{\times}\boldsymbol{J}_t\boldsymbol{\omega}_t = 0 \tag{5}$$

$$\boldsymbol{J}\dot{\boldsymbol{\omega}}_p + \boldsymbol{\omega}_p^{\times}\boldsymbol{J}\boldsymbol{\omega}_p = \boldsymbol{\tau} + \boldsymbol{\tau}_d \tag{6}$$

where $\boldsymbol{J} \in \mathbf{R}^{3\times 3}$ and $\boldsymbol{J}_t \in \mathbf{R}^{3\times 3}$ are the given inertia matrices of target and pursuer; $\boldsymbol{\tau} \in \mathbf{R}^3$ and $\boldsymbol{\tau}_d \in \mathbf{R}^3$ denote the control torque and the external disturbance torque, respectively.

The derivative of $\tilde{\boldsymbol{\omega}}$ can be calculated as:

$$\dot{\tilde{\boldsymbol{\omega}}} = \dot{\boldsymbol{\omega}}_p - \dot{\tilde{\boldsymbol{R}}}\boldsymbol{\omega}_t - \tilde{\boldsymbol{R}}\dot{\boldsymbol{\omega}}_t \tag{7}$$

Utilizing the fact that $\dot{\tilde{\boldsymbol{R}}} = \tilde{\boldsymbol{R}}\tilde{\boldsymbol{\omega}}^{\times}$ and combining Eqs. (5)-(7), we can conclude that

$$\boldsymbol{J}\dot{\tilde{\boldsymbol{\omega}}} = -\boldsymbol{C}_r\tilde{\boldsymbol{\omega}} - \boldsymbol{n}_r + \boldsymbol{\tau} + \boldsymbol{\tau}_d \tag{8}$$

where $\boldsymbol{C}_r = \boldsymbol{J}\left(\tilde{\boldsymbol{R}}\boldsymbol{\omega}_t\right)^{\times} + \left(\tilde{\boldsymbol{R}}\boldsymbol{\omega}_t\right)^{\times}\boldsymbol{J} - \left(\boldsymbol{J}\left(\tilde{\boldsymbol{\omega}} + \tilde{\boldsymbol{R}}\boldsymbol{\omega}_t\right)\right)^{\times}$ and $\boldsymbol{n}_r = \left(\tilde{\boldsymbol{R}}\boldsymbol{\omega}_t\right)^{\times}\boldsymbol{J}\tilde{\boldsymbol{R}}\boldsymbol{\omega}_t + \boldsymbol{J}\tilde{\boldsymbol{R}}\dot{\boldsymbol{\omega}}_t$.

B. RELATIVE ORBIT DYNAMICS MODEL

According to the relative motion between the pursuer and the target, the donation $\boldsymbol{r_p}$ and $\boldsymbol{v_p}$ are implemented to express the pursuer's position and velocity, respectively, which are expressed as [30]:

$$\boldsymbol{r_p} = \tilde{\boldsymbol{r}} + \tilde{\boldsymbol{R}}\left(\boldsymbol{r}_t + \boldsymbol{\delta}_t\right) \tag{9}$$

$$\boldsymbol{v_p} = \tilde{\boldsymbol{v}} + \tilde{\boldsymbol{R}}\left(\boldsymbol{v}_t + \boldsymbol{\omega}_t^{\times}\boldsymbol{\delta}_t\right) \tag{10}$$

where $\boldsymbol{\delta}_t \in R^3$ is the desired rendezvous position; $\boldsymbol{r}_t$ and $\boldsymbol{v}_t$ are the target's position and velocity; $\tilde{\boldsymbol{r}}$ and $\tilde{\boldsymbol{v}}$ are the relative position and velocity. By the calculation, one can obtain

$$\dot{\boldsymbol{r}}_{\boldsymbol{p}} = \dot{\tilde{\boldsymbol{r}}} + \dot{\tilde{\boldsymbol{R}}}\left(\boldsymbol{r}_t + \boldsymbol{\delta}_t\right) + \tilde{\boldsymbol{R}}\dot{\boldsymbol{r}}_t \tag{11}$$

Then, from the similar analysis in [28], the kinematics can be established as follows:

$$\dot{\boldsymbol{r}}_t = \boldsymbol{v}_t - \boldsymbol{\omega}_t^{\times}\boldsymbol{r}_t \tag{12}$$

$$\dot{\boldsymbol{r}}_{\boldsymbol{p}} = \boldsymbol{v_p} - \boldsymbol{\omega}_p^{\times}\boldsymbol{r_p} \tag{13}$$

Combining Eq. (11) and (13) yields

$$\boldsymbol{v_p} - \boldsymbol{\omega}_p^{\times}\boldsymbol{r_p} = \dot{\tilde{\boldsymbol{r}}} + \dot{\tilde{\boldsymbol{R}}}\left(\boldsymbol{r}_t + \boldsymbol{\delta}_t\right) + \tilde{\boldsymbol{R}}\dot{\boldsymbol{r}}_t \tag{14}$$

Based on the above analysis, the derivative of $\tilde{\boldsymbol{r}}$ will be given as Eq. (15) with $\boldsymbol{C}_t = \left(\tilde{\boldsymbol{\omega}} + \tilde{\boldsymbol{R}}\boldsymbol{\omega}_t\right)^{\times}$.

$$\dot{\tilde{\boldsymbol{r}}} = \tilde{\boldsymbol{v}} - \boldsymbol{C}_t\tilde{\boldsymbol{r}} \tag{15}$$

The derivative of Eq. (10) can be derived as

$$\dot{\boldsymbol{v}}_{\boldsymbol{p}} = \dot{\tilde{\boldsymbol{v}}} + \dot{\tilde{\boldsymbol{R}}}\left(\boldsymbol{v}_t + \boldsymbol{\omega}_t^{\times}\boldsymbol{\delta}_t\right) + \tilde{\boldsymbol{R}}\left(\dot{\boldsymbol{v}}_t + \dot{\boldsymbol{\omega}}_t^{\times}\boldsymbol{\delta}_t\right) \tag{16}$$

Through the theory in [28], the position dynamics can be established as follows:

$$m_t\dot{\boldsymbol{v}}_t + m_t\boldsymbol{\omega}_t^{\times}\boldsymbol{v}_t = \boldsymbol{0} \tag{17}$$

$$m_p\dot{\boldsymbol{v}}_p + m_p\boldsymbol{\omega}_p^{\times}\boldsymbol{v}_p = \boldsymbol{f} + \boldsymbol{f}_d \tag{18}$$

where m_t and m_p are constants defining masses of the target and the purser, respectively; $\boldsymbol{f} \in R^N$ and $\boldsymbol{f}_d \in R^3$ denote the control force and the external disturbance force. Combining Eq. (16) and (18), it follows that [30]

$$m_p\left[\dot{\tilde{\boldsymbol{v}}} + \dot{\tilde{\boldsymbol{R}}}\left(\boldsymbol{v}_t + \boldsymbol{\omega}_t^{\times}\delta_t\right) + \tilde{\boldsymbol{R}}\left(\dot{\boldsymbol{v}}_t + \dot{\boldsymbol{\omega}}_t^{\times}\delta_t\right)\right] + m_p\boldsymbol{\omega}_p^{\times}\boldsymbol{v}_p = \boldsymbol{f} + \boldsymbol{f}_d \tag{19}$$

That is

$$m_p\dot{\tilde{\boldsymbol{v}}} = -m_p\boldsymbol{C}_t\tilde{\boldsymbol{v}} - m_p\boldsymbol{n}_t + \boldsymbol{f} + \boldsymbol{f}_d \tag{20}$$

where $\boldsymbol{n}_t = \left(\tilde{\boldsymbol{R}}\boldsymbol{\omega}_t\right)^{\times}\tilde{\boldsymbol{R}}\boldsymbol{v}_t + \tilde{\boldsymbol{R}}\dot{\boldsymbol{v}}_t + \tilde{\boldsymbol{\omega}}^{\times}\tilde{\boldsymbol{R}}\delta_t^{\times}\boldsymbol{\omega}_t - \tilde{\boldsymbol{R}}\delta_t^{\times}\dot{\boldsymbol{\omega}}_t$.

In this paper, it is assumed that all the motion information of the target spacecraft can be provided to the tracker spacecraft by the measuring device. Then, the control objective of this paper is designing signals $\boldsymbol{\varepsilon}_r$ and $\boldsymbol{\varepsilon}_t$ for the dynamics expressed by Eqs. (8) and (20) such that finite-time stability of the close-loop system will be obtained with the control scheme.

For the purpose of facilitating the controller design, the following assumptions, lemmas and notations are given.

Assumption 1: The target spacecraft is stable. By using Eqs. (1), (2), (15) and (20) one can deduced that $\boldsymbol{\omega}_t$, $\dot{\boldsymbol{\omega}}_t$, $\boldsymbol{v}_t$, $\tilde{\boldsymbol{v}}_t$ all have upper bound which satisfying $\|\boldsymbol{\omega}_t\| \le a_1$, $\|\dot{\boldsymbol{\omega}}_t\| \le a_2$, $\|\boldsymbol{v}_t\| \le a_3$, $\|\tilde{\boldsymbol{v}}_t\| \le a_4$, where a_1, a_2, a_3, a_4 are unknown constants.

Assumption 2: $\boldsymbol{d}_r$are $\boldsymbol{d}_t$ unknown disturbances satisfying $\|\boldsymbol{d}_r\| \le D_r$, $\|\boldsymbol{d}_t\| \le D_t$, where D_r and D_t are positive constant.

Assumption 3: The inertia parameters $\boldsymbol{J}$ is unknown bounded and satisfying $\lambda_1\boldsymbol{I}_{3\times3} \le \boldsymbol{J} \le \lambda_2\boldsymbol{I}_{3\times3}$, where λ_1 and λ_2 are positive constants.

Lemma 1 [29]: For arbitrary real number $x \in R$, $\mu > 0$ and $\kappa = 0.2785$, the relation Eq. (25) exists.

$$0 < |x| - x\tanh(\mu x) \le \frac{\kappa}{\mu} \tag{21}$$

Lemma 2 [15]: For arbitrary positive constants $1 < \sigma < 2$ and ∂_i, $i = 1, 2, \ldots, n$, one can be obtained that

$$\left(\partial_1^2 + \cdots + \partial_n^2\right)^{\sigma} \le \left(\partial_1^{\sigma} + \cdots + \partial_n^{\sigma}\right)^2 \tag{22}$$

Lemma 3 [29]: For the system $\dot{x} = f(x)$, $f(0) = 0$, $x \in R^n$, $V(x)$ converges to the equilibrium point in finite time when the continuous function $V(x): U \to R$ satisfying Eq. (23), where $\gamma_1 > 0$, $0 < \gamma_2 < 1$.

$$\dot{V}(x) + \gamma_1 V^{\gamma_2}(x) \le 0 \tag{23}$$

Notations: The notation $\|\cdot\|$ denotes the Euclidean norm of a vector or the induced norm of a matrix. For arbitrary scalar $\xi \in R$, $\mathrm{sig}(\xi)^{\alpha}$ is introduced to represent $\mathrm{sig}(\xi)^{\alpha} = \left[\mathrm{sign}(\xi)|\xi|^{\alpha}\right]$. For a vector $\boldsymbol{\xi} = [\xi_1, \ldots, \xi_n]^{\mathrm{T}}$, $\mathrm{sig}(\boldsymbol{\xi})^{\alpha}$ is defined as $\mathrm{sig}(\boldsymbol{\xi})^{\alpha} = \left[\mathrm{sign}(\xi_1)|\xi_1|^{\alpha}, \ldots, \mathrm{sign}(\xi_n)|\xi_n|\right]^{\mathrm{T}}$.

III. CONTROL DESIGN

A. BASIC CONTROLLER DESIGN

In this section, two finite-time controllers for spacecraft rendezvous maneuver are synthesized via the combination of SMC and adaptive control when there exist external disturbances. Initially, a novel SMS has been proposed, which can ensure global finite-time convergence for the tracking errors. Furthermore, a basic control scheme is presented to guarantee that the SMS could be stabilized in finite time. Though it is effective for the rendezvous task, chattering problem is a threat to the safety of the actuators. Considering this drawback, a modified method is proposed in the second controller. As for the finite-time stability, the SMS will be redevised via adding a proportional term, which will be elaborated in the following part.

To develop the attitude and orbit control schemes, two sliding mode variables are defined as:

$$\boldsymbol{s}_1 = \dot{\tilde{\boldsymbol{q}}}_{\mathrm{v}} + k_1\tanh\left(\tilde{\boldsymbol{q}}_{\mathrm{v}}\right) \tag{24}$$

$$\boldsymbol{s}_2 = \dot{\tilde{\boldsymbol{r}}} + k_2\tanh\left(\tilde{\boldsymbol{r}}\right) \tag{25}$$

where k_1 and k_2 are positive constants. In consideration of Eqs. (2), (8), (15), (19), (24) and (25) mentioned above, the following relations of $\boldsymbol{s}_1$ and $\boldsymbol{s}_2$ can be obtained:

$$\begin{aligned}\boldsymbol{J}\dot{\boldsymbol{s}}_1 &= \boldsymbol{J}\ddot{\tilde{\boldsymbol{q}}}_v + k_1\boldsymbol{J}\left[1+\tanh^{\mathrm{T}}\left(\tilde{\boldsymbol{q}}_{\mathrm{v}}\right)\tanh\left(\tilde{\boldsymbol{q}}_{\mathrm{v}}\right)\right]\dot{\tilde{\boldsymbol{q}}}_v \\ &= \frac{1}{2}\boldsymbol{J}\left(\dot{\tilde{\boldsymbol{q}}}_v^{\times}+\dot{\tilde{q}}_0\boldsymbol{I}_3\right)\tilde{\boldsymbol{\omega}}+\frac{1}{2}\left(\tilde{\boldsymbol{q}}_v^{\times}+\tilde{q}_0\boldsymbol{I}_3\right) \\ &\quad\times\left(-\boldsymbol{C}_r\tilde{\boldsymbol{\omega}}-\boldsymbol{n}_r+\boldsymbol{\varepsilon}_r+\boldsymbol{d}_r\right) \\ &\quad+k_1\boldsymbol{J}\left[1+\tanh^{\mathrm{T}}\left(\tilde{\boldsymbol{q}}_{\mathrm{v}}\right)\tanh\left(\tilde{\boldsymbol{q}}_{\mathrm{v}}\right)\right]\dot{\tilde{\boldsymbol{q}}}_v \qquad (26)\\ m\dot{\boldsymbol{s}}_2 &= m\left\{\ddot{\tilde{\boldsymbol{r}}}+k_2\left[1+\tanh^{\mathrm{T}}\left(\tilde{\boldsymbol{r}}\right)\tanh\left(\tilde{\boldsymbol{r}}\right)\right]\dot{\tilde{\boldsymbol{r}}}\right\} \\ &= m\dot{\tilde{\boldsymbol{v}}}-m\boldsymbol{C}_t\ddot{\tilde{\boldsymbol{r}}}-m\dot{\boldsymbol{C}}_t\dot{\tilde{\boldsymbol{r}}} \\ &\quad+mk_2\left[1+\tanh^{\mathrm{T}}\left(\tilde{\boldsymbol{r}}\right)\tanh\left(\tilde{\boldsymbol{r}}\right)\right]\dot{\tilde{\boldsymbol{r}}} \\ &= -m\boldsymbol{C}_t\tilde{\boldsymbol{v}}-m\boldsymbol{n}_t+\boldsymbol{\varepsilon}_t+\boldsymbol{d}_t-m\boldsymbol{C}_t\dot{\tilde{\boldsymbol{r}}}-m\dot{\boldsymbol{C}}_t\tilde{\boldsymbol{r}} \\ &\quad+mk_2\left[1+\tanh^{\mathrm{T}}\left(\tilde{\boldsymbol{r}}\right)\tanh\left(\tilde{\boldsymbol{r}}\right)\right]\dot{\tilde{\boldsymbol{r}}} \\ &= -m\boldsymbol{C}_t\tilde{\boldsymbol{v}}-m\boldsymbol{n}_t+\boldsymbol{\varepsilon}_t+\boldsymbol{d}_t-m\boldsymbol{C}_t\dot{\tilde{\boldsymbol{r}}} \\ &\quad-m\dot{\boldsymbol{C}}_t\tilde{\boldsymbol{r}}+k_2\left[1+\tanh^{\mathrm{T}}\left(\tilde{\boldsymbol{r}}\right)\tanh\left(\tilde{\boldsymbol{r}}\right)\right]\dot{\tilde{\boldsymbol{r}}} \qquad (27)\end{aligned}$$

Control laws for attitude and orbit tracking systems can be developed as

$$\begin{aligned}\boldsymbol{\varepsilon}_r &= \boldsymbol{C}_r\tilde{\boldsymbol{\omega}}+\boldsymbol{n}_r-2\left(\tilde{\boldsymbol{q}}_v^{\times}+\tilde{q}_0\boldsymbol{I}_3\right)^{-1} \\ &\quad\times\left[k_3\mathrm{sign}\left(\boldsymbol{s}_1\right)+k_4\boldsymbol{s}_1+\frac{\boldsymbol{s}_1\hat{D}_r}{2\left\|\boldsymbol{s}_1\right\|}\right] \\ &\quad-2\left(\tilde{\boldsymbol{q}}_v^{\times}+\tilde{q}_0\boldsymbol{I}_3\right)^{-1}\boldsymbol{J}\left[\frac{1}{2}\left(\dot{\tilde{\boldsymbol{q}}}_v^{\times}+\dot{\tilde{q}}_0\boldsymbol{I}_3\right)\tilde{\boldsymbol{\omega}}\right. \\ &\quad\left.+k_1\left(1+\tanh^{\mathrm{T}}\left(\tilde{\boldsymbol{q}}_{\mathrm{v}}\right)\tanh\left(\tilde{\boldsymbol{q}}_{\mathrm{v}}\right)\right)\dot{\tilde{\boldsymbol{q}}}_v\right] \qquad (28)\\ \boldsymbol{\varepsilon}_t &= m\boldsymbol{C}_t\tilde{\boldsymbol{v}}+m\boldsymbol{n}_t+m\boldsymbol{C}_t\dot{\tilde{\boldsymbol{r}}}+m\dot{\boldsymbol{C}}_t\tilde{\boldsymbol{r}} \\ &\quad-k_2m\left[1+\tanh^{\mathrm{T}}\left(\tilde{\boldsymbol{r}}\right)\tanh\left(\tilde{\boldsymbol{r}}\right)\right]\dot{\tilde{\boldsymbol{r}}} \\ &\quad-k_5\mathrm{sign}\left(\boldsymbol{s}_2\right)-k_6\boldsymbol{s}_2-\frac{\boldsymbol{s}_2\hat{D}_t}{\left\|\boldsymbol{s}_2\right\|} \qquad (29)\end{aligned}$$

where $k_i>0$, $i=3,4,5,6$, $\hat{D}_r$ and $\hat{D}_t$ are estimations of D_r and D_t, respectively. The definition of $\hat{D}_r$ and $\hat{D}_t$ are given as follows:

$$\dot{\hat{D}}_r = \frac{c_1\left\|\boldsymbol{s}_1\right\|}{2} \qquad (30)$$

$$\dot{\hat{D}}_t = c_2\left\|\boldsymbol{s}_2\right\| \qquad (31)$$

where $c_i>0$, $i=1,2,$. The estimation errors are defined as:

$$\tilde{D}_r = D_r-\hat{D}_r \qquad (32)$$

$$\dot{\tilde{D}}_t = D_t-\hat{D}_t \qquad (33)$$

Remark 1: In Eqs. (24)-(25), the SMS is proposed by resorting the hyperbolic tangent function, which will ensure finite-time stability for the tracking error systems. Comparing with the existing sliding mode methods [13]–[16], the proposed possesses the advantage of simplicity and non-singularity.

Remark 2: Global finite-time convergence is achievable for tracking errors $\tilde{\boldsymbol{q}}_{\mathrm{v}}$ and $\tilde{\boldsymbol{r}}$, which will improve the convergence rate for spacecraft rendezvous maneuver missions.

Based on the foregoing illustration, the following conclusion is obtained:

Theorem 1: For the spacecraft tracking control system Eqs. (1), (2), (8), (15) and (20) satisfying Assumptions 1-3, finite-time convergence for tracking errors $\tilde{\boldsymbol{q}}_{\mathrm{v}}$ and $\tilde{\boldsymbol{r}}$ is achievable when the control laws are devised as Eqs. (28)-(31). Additionally, the estimation errors $\tilde{D}_r$and $\tilde{D}_t$ are uniformly ultimately bounded.

Proof: To show the stability of the entire system, the Lyapunov function (LF) is given as follows:

$$V_1 = \frac{1}{2}\boldsymbol{s}_1^{\mathrm{T}}\boldsymbol{J}\boldsymbol{s}_1+\frac{1}{2}\boldsymbol{s}_2^{\mathrm{T}}m\boldsymbol{s}_2+\frac{1}{2c_1}\tilde{D}_r^2+\frac{1}{2c_2}\tilde{D}_t^2 \qquad (34)$$

Upon the utilization of the relevant system dynamics and control laws, the derivative of $\boldsymbol{V}_1$ is calculated as follows:

$$\begin{aligned}\dot{V}_1 &= \boldsymbol{s}_1^{\mathrm{T}}\boldsymbol{J}\dot{\boldsymbol{s}}_1+\boldsymbol{s}_2^{\mathrm{T}}m\dot{\boldsymbol{s}}_2+\frac{1}{c_1}\tilde{D}_r\dot{\tilde{D}}_r+\frac{1}{c_2}\tilde{D}_t\dot{\tilde{D}}_t \\ &= \boldsymbol{s}_1^{\mathrm{T}}\left[\frac{1}{2}\boldsymbol{J}\left(\dot{\tilde{\boldsymbol{q}}}_v^{\times}+\dot{\tilde{q}}_0\boldsymbol{I}_3\right)\tilde{\boldsymbol{\omega}}+\frac{1}{2}\left(\tilde{\boldsymbol{q}}_v^{\times}+\tilde{q}_0\boldsymbol{I}_3\right)\right. \\ &\quad\times\left(-\boldsymbol{C}_r\tilde{\boldsymbol{\omega}}-\boldsymbol{n}_r+\boldsymbol{\varepsilon}_r+\boldsymbol{\tau}_d\right) \\ &\quad\left.+k_1\boldsymbol{J}\left(1+\tanh^{\mathrm{T}}\left(\tilde{\boldsymbol{q}}_{\mathrm{v}}\right)\tanh\left(\tilde{\boldsymbol{q}}_{\mathrm{v}}\right)\right)\dot{\tilde{\boldsymbol{q}}}_v\right] \\ &\quad+\boldsymbol{s}_2^{\mathrm{T}}\left[-m\boldsymbol{C}_t\tilde{\boldsymbol{v}}-m\boldsymbol{n}_t+\boldsymbol{\varepsilon}_t+\boldsymbol{f}_d-m\boldsymbol{C}_t\dot{\tilde{\boldsymbol{r}}}\right. \\ &\quad\left.-m\dot{\boldsymbol{C}}_t\tilde{\boldsymbol{r}}+k_2m\left(1+\tanh^{\mathrm{T}}\left(\tilde{\boldsymbol{r}}\right)\tanh\left(\tilde{\boldsymbol{r}}\right)\right)\dot{\tilde{\boldsymbol{r}}}\right] \\ &\quad-\frac{1}{c_1}\tilde{D}_r\dot{\tilde{D}}_r-\frac{1}{c_2}\tilde{D}_t\dot{\tilde{D}}_t \\ &= \boldsymbol{s}_1^{\mathrm{T}}\left(\frac{1}{2}\left(\tilde{\boldsymbol{q}}_{\mathrm{v}}^{\times}+\tilde{q}_0\boldsymbol{I}_3\right)\boldsymbol{\tau}_d-k_3\mathrm{sign}\left(\boldsymbol{s}_1\right)\right. \\ &\quad\left.-k_4\boldsymbol{s}_1-\frac{\boldsymbol{s}_1\hat{D}_r}{2\left\|\boldsymbol{s}_1\right\|}\right)+\boldsymbol{s}_2^{\mathrm{T}}\left(\boldsymbol{f}_d-k_5\mathrm{sign}\left(\boldsymbol{s}_2\right)\right. \\ &\quad\left.-k_6\boldsymbol{s}_2-\frac{\boldsymbol{s}_2\hat{D}_t}{\left\|\boldsymbol{s}_2\right\|}\right)-\frac{1}{c_1}\tilde{D}_r\dot{\tilde{D}}_r-\frac{1}{c_2}\tilde{D}_t\dot{\tilde{D}}_t \\ &\leq \frac{\left\|\boldsymbol{s}_1\right\|}{2}D_r-k_3\left\|\boldsymbol{s}_1\right\|-k_4\left\|\boldsymbol{s}_1\right\|^2-\frac{\left\|\boldsymbol{s}_1\right\|}{2}\hat{D}_r+\left\|\boldsymbol{s}_2\right\|D_t \\ &\quad-k_5\left\|\boldsymbol{s}_2\right\|-k_6\left\|\boldsymbol{s}_2\right\|^2-\left\|\boldsymbol{s}_2\right\|\hat{D}_t-\frac{1}{c_1}\tilde{D}_r\dot{\tilde{D}}_r-\frac{1}{c_2}\tilde{D}_t\dot{\tilde{D}}_t \\ &= \frac{\left\|\boldsymbol{s}_1\right\|}{2}\tilde{D}_r-k_3\left\|\boldsymbol{s}_1\right\|-k_4\left\|\boldsymbol{s}_1\right\|^2-\frac{1}{c_1}\tilde{D}_r\dot{\tilde{D}}_r+\left\|\boldsymbol{s}_2\right\|\tilde{D}_t \\ &\quad-k_5\left\|\boldsymbol{s}_2\right\|-k_6\left\|\boldsymbol{s}_2\right\|^2-\frac{1}{c_2}\tilde{D}_t\dot{\tilde{D}}_t \qquad (35)\end{aligned}$$

Inserting Eqs. (30)-(31), Eq. (35) is further obtained as:

$$\begin{aligned}\dot{V}_1 &\leq -k_3\left\|\boldsymbol{s}_1\right\|-k_4\left\|\boldsymbol{s}_1\right\|^2-k_5\left\|\boldsymbol{s}_2\right\|-k_6\left\|\boldsymbol{s}_2\right\|^2 \\ &\leq 0 \qquad (36)\end{aligned}$$

which implies $\boldsymbol{s}_1$, $\boldsymbol{s}_2$, $\tilde{D}_r$, $\tilde{D}_t$ are uniformly ultimately bounded. Thus, there must exist two constants$\bar{D}_r$ and $\bar{D}_r$ satisfying $\bar{D}_r \geq D_r, \bar{D}_r \geq \hat{D}_r, \bar{D}_t \geq D_t, \bar{D}_t \geq \hat{D}_t$.

Then, the following LF is presented:

$$V_2 = \frac{1}{2}\boldsymbol{s}_1^{\mathrm{T}}\boldsymbol{J}\boldsymbol{s}_1 + \frac{1}{2}\boldsymbol{s}_2^{\mathrm{T}} m \boldsymbol{s}_2 + \frac{1}{c_1}\left(\bar{D}_r - \hat{D}_r\right)^2 + \frac{1}{c_2}\left(\bar{D}_t - \hat{D}_t\right)^2 \tag{37}$$

The derivative of V_2 is derived as:

$$\begin{aligned}
\dot{V}_2 =& \boldsymbol{s}_1^{\mathrm{T}}\boldsymbol{J}\dot{\boldsymbol{s}}_1 + \boldsymbol{s}_2^{\mathrm{T}} m \dot{\boldsymbol{s}}_2 - \frac{2}{c_1}\left(\bar{D}_r - \hat{D}_r\right)\dot{\hat{D}}_r - \frac{2}{c_2}\left(\bar{D}_t - \hat{D}_t\right)\dot{\hat{D}}_t \\
=& \boldsymbol{s}_1^{\mathrm{T}}\left[\frac{1}{2}\boldsymbol{J}\left(\dot{\tilde{\boldsymbol{q}}}_v^{\times} + \dot{\tilde{q}}_0\boldsymbol{I}_3\right)\tilde{\boldsymbol{\omega}} + \frac{1}{2}\left(\tilde{\boldsymbol{q}}_v^{\times} + \tilde{q}_0\boldsymbol{I}_3\right)\right. \\
& \times\left(-\boldsymbol{C}_r\tilde{\boldsymbol{\omega}} - \boldsymbol{n}_r + \boldsymbol{\varepsilon}_r + \boldsymbol{\tau}_d\right) \\
& \left. + k_1\boldsymbol{J}\left(1 + \tanh^{\mathrm{T}}\left(\tilde{\boldsymbol{q}}_{\mathrm{v}}\right)\tanh\left(\tilde{\boldsymbol{q}}_{\mathrm{v}}\right)\right)\dot{\tilde{\boldsymbol{q}}}_v\right] \\
& + \boldsymbol{s}_2^{\mathrm{T}}\left[-m\boldsymbol{C}_t\tilde{\boldsymbol{v}} - m\boldsymbol{n}_t + \boldsymbol{f}_d - m\boldsymbol{C}_t\dot{\tilde{\boldsymbol{r}}}\right. \\
& \left. - m\dot{\boldsymbol{C}}_t\tilde{\boldsymbol{r}} + k_2\left(1 + \tanh^{\mathrm{T}}\left(\tilde{\boldsymbol{r}}\right)\tanh\left(\tilde{\boldsymbol{r}}\right)\right)\dot{\tilde{\boldsymbol{r}}}\right] \\
& - \frac{2}{c_1}\left(\bar{D}_r - \hat{D}_r\right)\dot{\hat{D}}_r - \frac{2}{c_2}\left(\bar{D}_t - \hat{D}_t\right)\dot{\hat{D}}_t \\
=& \boldsymbol{s}_1^{\mathrm{T}}\left(\frac{1}{2}\left(\tilde{\boldsymbol{q}}_{\mathrm{v}}^{\times} + \tilde{q}_0\boldsymbol{I}_3\right)\boldsymbol{\tau}_d - k_3\mathrm{sign}\left(\boldsymbol{s}_1\right)\right. \\
& \left. - k_4\boldsymbol{s}_1 - \frac{\boldsymbol{s}_1\hat{D}_r}{2\left\|\boldsymbol{s}_1\right\|}\right) + \boldsymbol{s}_2^{\mathrm{T}}\left(\boldsymbol{f}_d - k_5\mathrm{sign}\left(\boldsymbol{s}_2\right)\right. \\
& \left. - k_6\boldsymbol{s}_2 - \frac{\boldsymbol{s}_2\hat{D}_t}{\left\|\boldsymbol{s}_2\right\|}\right) - \frac{2}{c_1}\left(\bar{D}_r - \hat{D}_r\right)\dot{\hat{D}}_r - \frac{2}{c_2}\left(\bar{D}_t - \hat{D}_t\right)\dot{\hat{D}}_t \\
\leq& \frac{\left\|\boldsymbol{s}_1\right\|}{2}\left(D_r - \hat{D}_r\right) - k_3\left\|\boldsymbol{s}_1\right\| - k_4\left\|\boldsymbol{s}_1\right\|^2 + \left\|\boldsymbol{s}_2\right\|\left(D_t - \hat{D}_t\right) \\
& - k_5\left\|\boldsymbol{s}_2\right\| - k_6\left\|\boldsymbol{s}_2\right\|^2 - \left\|\boldsymbol{s}_2\right\|\hat{D}_t - \left(\bar{D}_r - \hat{D}_r\right)\left\|\boldsymbol{s}_1\right\| \\
& - 2\left(\bar{D}_t - \hat{D}_t\right)\left\|\boldsymbol{s}_2\right\|
\end{aligned} \tag{38}$$

According to the fact that $\bar{D}_r \geq D_r$, $\bar{D}_r \geq \hat{D}_r$, $\bar{D}_t \geq D_t$, $\bar{D}_t \geq \hat{D}_t$, Eq. (38) is rearranged as:

$$\begin{aligned}
\dot{V}_2 \leq& -k_3\left\|\boldsymbol{s}_1\right\| - k_4\left\|\boldsymbol{s}_1\right\|^2 - k_5\left\|\boldsymbol{s}_2\right\| - k_6\left\|\boldsymbol{s}_2\right\|^2 \\
& - \left(\bar{D}_r - \hat{D}_r\right)\frac{\left\|\boldsymbol{s}_1\right\|}{2} - \left(\bar{D}_t - \hat{D}_t\right)\left\|\boldsymbol{s}_2\right\| \\
\leq& -\rho_1 V_2^{\frac{1}{2}}
\end{aligned} \tag{39}$$

where $\rho_1 = \min\left(\frac{\sqrt{c_1}\left\|\boldsymbol{s}_1\right\|}{2}, \sqrt{c_2}\left\|\boldsymbol{s}_2\right\|, k_3\sqrt{\frac{2}{\lambda_2}}, k_5\sqrt{\frac{2}{m}}\right)$. According to Lemma 3, we conclude that the SMS $\boldsymbol{s}_1$ and $\boldsymbol{s}_2$ converge to the origin in finite time.

When the SMS $\boldsymbol{s}_1 = 0, \boldsymbol{s}_2 = 0$ is reached, it implies:

$$\dot{\tilde{\boldsymbol{q}}}_{\mathrm{v}} + k_1\tanh\left(\tilde{\boldsymbol{q}}_{\mathrm{v}}\right) = 0 \tag{40}$$

$$\dot{\tilde{\boldsymbol{r}}} + k_2\tanh\left(\tilde{\boldsymbol{r}}\right) = 0 \tag{41}$$

The stability of $\tilde{\boldsymbol{q}}_{\mathrm{v}}$ and $\tilde{\boldsymbol{r}}$ can be validated by reselecting a LF as following:

$$V_3 = \frac{1}{2}\tilde{\boldsymbol{q}}_v^{\mathrm{T}}\tilde{\boldsymbol{q}}_v + \frac{1}{2}\tilde{\boldsymbol{r}}^{\mathrm{T}}\tilde{\boldsymbol{r}} \tag{42}$$

Utilizing Eqs. (40)-(41), $\dot{V}_3$ satisfies:

$$\begin{aligned}
\dot{V}_3 =& \tilde{\boldsymbol{q}}_v^{\mathrm{T}}\dot{\tilde{\boldsymbol{q}}}_v + \tilde{\boldsymbol{r}}^{\mathrm{T}}\dot{\tilde{\boldsymbol{r}}} \\
=& -k_1\tilde{\boldsymbol{q}}_v^{\mathrm{T}}\tanh\left(\tilde{\boldsymbol{q}}_{\mathrm{v}}\right) - k_2\tilde{\boldsymbol{r}}^{\mathrm{T}}\tanh\left(\tilde{\boldsymbol{r}}\right)
\end{aligned} \tag{43}$$

In terms of Lemma 1, Eq. (43) is equivalent to the following equation:

$$\begin{aligned}
\dot{V}_3 \leq& -k_1\sum_{i=1}^{3}\left|\tilde{q}_{vi}\right| - k_2\sum_{i=1}^{3}\left|\tilde{r}_i\right| + 3\left(k_1 + k_2\right)\kappa \\
\leq& -\rho_2 V_3^{\frac{1}{2}} + 3\left(k_1 + k_2\right)\kappa
\end{aligned} \tag{44}$$

where $\rho_2 = \min\left(\sqrt{2}\,k_1, \sqrt{2}\,k_2\right)$. Consequently, $\tilde{\boldsymbol{q}}_{\mathrm{v}}$ and $\tilde{\boldsymbol{r}}$ will converge to a compact set defined as $\left\{\left(\tilde{\boldsymbol{q}}_v, \tilde{\boldsymbol{r}}\right) \middle| \left\|\tilde{\boldsymbol{q}}_v\right\| \leq 3\sqrt{2}\left(k_1 + k_2\right)\kappa, \left\|\tilde{\boldsymbol{r}}\right\| \leq 3\sqrt{2}\left(k_1 + k_2\right)\kappa\right\}$ in finite time.

Thus, it completes the proof of Theorem 1.

B. CHATTERING-FREE CONTROLLER DESIGN

As a matter of fact, the so-called chattering problem will be introduced by controller Eqs. (28)-(31). Additionally, by observing the definitions of the adaptive laws expressed by Eqs. (30)-(31), it is found that $\hat{D}_r$ and $\hat{D}_t$ tends to infinity when time goes infinite as long as their initial values satisfy $\hat{D}_r(0) > 0$ and $\hat{D}_t(0) > 0$. To overcome these two disadvantages, the SMS and the corresponding control laws are redesigned as follows:

$$\boldsymbol{s}_1 = \dot{\tilde{\boldsymbol{q}}}_{\mathrm{v}} + k_1\tilde{\boldsymbol{q}}_{\mathrm{v}} + k_2\tanh\left(\tilde{\boldsymbol{q}}_{\mathrm{v}}\right) \tag{45}$$

$$\boldsymbol{s}_2 = \dot{\tilde{\boldsymbol{r}}} + k_3\tilde{\boldsymbol{r}} + k_4\tanh\left(\tilde{\boldsymbol{r}}\right) \tag{46}$$

$$\begin{aligned}
\boldsymbol{\varepsilon}_r =& \boldsymbol{C}_r\tilde{\boldsymbol{\omega}} + \boldsymbol{n}_r - 2\left(\tilde{\boldsymbol{q}}_v^{\times} + \tilde{q}_0\boldsymbol{I}_3\right)^{-1} \\
& \times\left[k_5\mathrm{sig}^{\gamma_1}\left(\boldsymbol{s}_1\right) + k_6\boldsymbol{s}_1 + \frac{\hat{D}_r\boldsymbol{s}_1}{2\left\|\boldsymbol{s}_1\right\| + \varepsilon_1}\right] \\
& - 2\left(\tilde{\boldsymbol{q}}_v^{\times} + \tilde{q}_0\boldsymbol{I}_3\right)^{-1}\boldsymbol{J}\left[\frac{1}{2}\left(\tilde{\boldsymbol{q}}_v^{\times} + \dot{\tilde{q}}_0\boldsymbol{I}_3\right)\tilde{\boldsymbol{\omega}}\right. \\
& \left. + k_2\left(1 + \tanh^{\mathrm{T}}\left(\tilde{\boldsymbol{q}}_{\mathrm{v}}\right)\tanh\left(\tilde{\boldsymbol{q}}_{\mathrm{v}}\right)\right)\dot{\tilde{\boldsymbol{q}}}_v + k_1\dot{\tilde{\boldsymbol{q}}}_v\right]
\end{aligned} \tag{47}$$

$$\begin{aligned}
\boldsymbol{\varepsilon}_t =& m\boldsymbol{C}_t\tilde{\boldsymbol{v}} + m\boldsymbol{n}_t + m\boldsymbol{C}_t\dot{\tilde{\boldsymbol{r}}} + m\dot{\boldsymbol{C}}_t\tilde{\boldsymbol{r}} \\
& - k_4 m\left[1 + \tanh^{\mathrm{T}}\left(\tilde{\boldsymbol{r}}\right)\tanh\left(\tilde{\boldsymbol{r}}\right)\right]\dot{\tilde{\boldsymbol{r}}} \\
& - k_7\mathrm{sig}^{\gamma_2}\left(\boldsymbol{s}_2\right) - k_8\boldsymbol{s}_2 - \frac{\hat{D}_t\boldsymbol{s}_2}{\left\|\boldsymbol{s}_2\right\| + \varepsilon_2} - k_3 m\dot{\tilde{\boldsymbol{r}}}
\end{aligned} \tag{48}$$

$$\varepsilon_1 = \frac{k_9}{1 + \hat{D}_r} \tag{49}$$

$$\varepsilon_2 = \frac{k_{10}}{1 + \hat{D}_t} \tag{50}$$

$$\dot{\hat{D}}_r = \mathrm{c}_1\left(\frac{\left\|\boldsymbol{s}_1\right\|}{2} - c_3\hat{D}_r\right) \tag{51}$$

$$\dot{\hat{D}}_t = c_2\left(\left\|\boldsymbol{s}_2\right\| - c_4\hat{D}_t\right) \tag{52}$$

where k_i, $i = 1, 2, \ldots, 10$ are positive constants satisfying $k_1 > 1, k_3 > 1, c_j > 0, j = 1, 2, 3, 4$.

Remark 3: To handle the chattering problem, terms $\frac{s_1\hat{D}_r}{2\|s_1\|}$ and $\frac{s_2\hat{D}_t}{\|s_2\|}$ in Eqs. (28)-(29) are replaced by $\frac{\hat{D}_r s_1}{2\|s_1\|+\varepsilon_1}$ and $\frac{\hat{D}_t s_2}{\|s_2\|+\varepsilon_2}$, respectively; $k_3\text{sign}(s_1)$ and $k_5\text{sign}(s_2)$ are replaced by $k_5\text{sig}^{\gamma_1}(s_1)$ and $k_7\text{sig}^{\gamma_2}(s_2)$. In this way, the chattering phenomenon will be reduced extensively.

Remark 4: Compared with the SMS proposed in Eqs. (24)-(25), proportional terms are added in Eqs. (45)-(46), which are used for enhancing the robustness of the controller and ensuring finite-time stability for the tracking errors when the SMS can only be stabilized to a compact set rather than zero.

Remark 5: By introducing proportional terms $c_3\hat{D}_r$ and $c_4\hat{D}_t$ in the adaptive laws Eqs. (51)-(52), estimations of $\hat{D}_r$ and $c_4\hat{D}_t$ will not tends to infinity. Thus, the mentioned drawback in the basic controller will be improved.

Theorem 2: For the spacecraft tracking control system Eqs. (1), (2), (8), (15) and (20) satisfying Assumptions 1-3, tracking errors $\tilde{\boldsymbol{q}}_v$ and $\tilde{\boldsymbol{r}}$ will be stabilized to a compact set in finite time when the control laws are devised as Eqs. (47)-(52). Additionally, the estimation errors $\tilde{D}_r$ and $\tilde{D}_t$ are uniformly ultimately bounded.

Proof: To demonstrate convergence of the sliding mode surface, the following LF is selected:

$$V_4 = \frac{1}{2}\boldsymbol{s}_1^{\mathrm{T}}\boldsymbol{J}\boldsymbol{s}_1 + \frac{1}{2}\boldsymbol{s}_2^{\mathrm{T}}m\boldsymbol{s}_2 + \frac{1}{2c_1}\tilde{D}_r^2 + \frac{1}{2c_2}\tilde{D}_t^2 \tag{53}$$

By taking the derivative of V_1 and utilizing the proposed control scheme Eqs. (45)-(50), one has:

$$\begin{aligned}
\dot{V}_4 &= \boldsymbol{s}_1^{\mathrm{T}}\boldsymbol{J}\dot{\boldsymbol{s}}_1 + \boldsymbol{s}_2^{\mathrm{T}}m\dot{\boldsymbol{s}}_2 + \frac{1}{c_1}\tilde{D}_r\dot{\tilde{D}}_r + \frac{1}{c_2}\tilde{D}_t\dot{\tilde{D}}_t \\
&= \boldsymbol{s}_1^{\mathrm{T}}\Bigg[\frac{1}{2}\boldsymbol{J}\left(\dot{\tilde{\boldsymbol{q}}}_v^{\times} + \dot{\tilde{q}}_0\boldsymbol{I}_3\right)\tilde{\boldsymbol{\omega}} + \frac{1}{2}\left(\tilde{\boldsymbol{q}}_v^{\times} + \tilde{q}_0\boldsymbol{I}_3\right) \\
&\quad \times\left(-\boldsymbol{C}_r\tilde{\boldsymbol{\omega}} - \boldsymbol{n}_r + \boldsymbol{\varepsilon}_r + \boldsymbol{\tau}_d\right) \\
&\quad + k_2\boldsymbol{J}\left(1 + \tanh^{\mathrm{T}}\left(\tilde{\boldsymbol{q}}_v\right)\tanh\left(\tilde{\boldsymbol{q}}_v\right)\right)\dot{\tilde{\boldsymbol{q}}}_v + k_1\dot{\tilde{\boldsymbol{q}}}_v\Bigg] \\
&\quad + \boldsymbol{s}_2^{\mathrm{T}}\Big[-m\boldsymbol{C}_t\tilde{\boldsymbol{v}} - m\boldsymbol{n}_t + \boldsymbol{\varepsilon}_t + \boldsymbol{f}_d - m\boldsymbol{C}_t\dot{\tilde{\boldsymbol{r}}} + k_3m\dot{\tilde{\boldsymbol{r}}} \\
&\quad - m\dot{\boldsymbol{C}}_t\tilde{\boldsymbol{r}} + k_4m\left(1 + \tanh^{\mathrm{T}}\left(\tilde{\boldsymbol{r}}\right)\tanh\left(\tilde{\boldsymbol{r}}\right)\right)\dot{\tilde{\boldsymbol{r}}}\Big] \\
&\quad - \frac{1}{c_1}\tilde{D}_r\dot{\tilde{D}}_r - \frac{1}{c_2}\tilde{D}_t\dot{\tilde{D}}_t \\
&= \boldsymbol{s}_1^{\mathrm{T}}\Bigg(\frac{1}{2}\left(\tilde{\boldsymbol{q}}_{\mathrm{v}}^{\times} + \tilde{q}_0\boldsymbol{I}_3\right)\boldsymbol{\tau}_d - k_5\text{sig}^{\gamma_1}(\boldsymbol{s}_1) - k_6\boldsymbol{s}_1 \\
&\quad - \frac{\hat{D}_r\boldsymbol{s}_1}{2\|\boldsymbol{s}_1\| + \varepsilon_1}\Bigg) + \boldsymbol{s}_2^{\mathrm{T}}\Bigg(\boldsymbol{f}_d - k_7\text{sig}^{\gamma_2}(\boldsymbol{s}_2) \\
&\quad - k_8\boldsymbol{s}_2 - \frac{\hat{D}_t\boldsymbol{s}_2}{\|\boldsymbol{s}_2\| + \varepsilon_2}\Bigg) - \frac{1}{c_1}\tilde{D}_r\dot{\tilde{D}}_r - \frac{1}{c_2}\tilde{D}_t\dot{\tilde{D}}_t
\end{aligned} \tag{54}$$

Noting that terms $\boldsymbol{s}_1^{\mathrm{T}}\frac{\boldsymbol{s}_1\hat{D}_r}{2\|\boldsymbol{s}_1\|+\varepsilon_1}$ and $\boldsymbol{s}_2^{\mathrm{T}}\frac{\hat{D}_t\boldsymbol{s}_2}{\|\boldsymbol{s}_2\|+\varepsilon_2}$ satisfy the following relation:

$$\begin{aligned}
-\boldsymbol{s}_1^{\mathrm{T}}\frac{\boldsymbol{s}_1\hat{D}_r}{2\|\boldsymbol{s}_1\| + \varepsilon_1} &= -\hat{D}_r\frac{\|\boldsymbol{s}_1\|}{2} + \left(\frac{\hat{D}_r\varepsilon_1}{2}\right)\frac{\|\boldsymbol{s}_1\|}{2\|\boldsymbol{s}_1\| + \varepsilon_1} \\
&= -\hat{D}_r\|\boldsymbol{s}_1\| + \frac{k_9\hat{D}_r}{2\left(1 + \hat{D}_r\right)} \times \frac{\|\boldsymbol{s}_1\|}{\|\boldsymbol{s}_1\| + \varepsilon_1} \\
&\le -\hat{D}_r\|\boldsymbol{s}_1\| + \frac{k_9}{2}
\end{aligned} \tag{55}$$

$$\begin{aligned}
-\boldsymbol{s}_2^{\mathrm{T}}\frac{\hat{D}_t\boldsymbol{s}_2}{\|\boldsymbol{s}_2\| + \varepsilon_2} &= -\hat{D}_t\|\boldsymbol{s}_2\| + \left(\hat{D}_t\varepsilon_2\right)\frac{\|\boldsymbol{s}_2\|}{\|\boldsymbol{s}_2\| + \varepsilon_2} \\
&= -\hat{D}_t\|\boldsymbol{s}_2\| + \frac{k_{10}\hat{D}_t}{1 + \hat{D}_t} \times \frac{\|\boldsymbol{s}_2\|}{\|\boldsymbol{s}_2\| + \varepsilon_2} \\
&\le -\hat{D}_t\|\boldsymbol{s}_2\| + k_{10}
\end{aligned} \tag{56}$$

Substituting Eqs. (55)-(56) into Eq. (54), one has:

$$\begin{aligned}
\dot{V}_4 \le\ & \frac{\|\boldsymbol{s}_1\|}{2}D_r - \boldsymbol{s}_1^{\mathrm{T}}\Bigg(k_5\text{sig}^{\gamma_1}(\boldsymbol{s}_1) + k_6\boldsymbol{s}_1 \\
&+ \frac{\hat{D}_r\boldsymbol{s}_1}{2\|\boldsymbol{s}_1\| + \varepsilon_1}\Bigg) + \|\boldsymbol{s}_2\|\tilde{D}_t - \boldsymbol{s}_2^{\mathrm{T}}\Bigg(k_7\text{sig}^{\gamma_2}(\boldsymbol{s}_2) \\
&+ k_8\boldsymbol{s}_2 + \frac{\hat{D}_t\boldsymbol{s}_2}{\|\boldsymbol{s}_2\| + \varepsilon_2}\Bigg) - \frac{1}{c_1}\tilde{D}_r\dot{\tilde{D}}_r - \frac{1}{c_2}\tilde{D}_t\dot{\tilde{D}}_t \\
\le\ & \frac{\|\boldsymbol{s}_1\|}{2}\tilde{D}_t - k_5\boldsymbol{s}_1^{\mathrm{T}}\text{sig}^{\gamma_1}(\boldsymbol{s}_1) - k_6\boldsymbol{s}_1^{\mathrm{T}}\boldsymbol{s}_1 \\
&+ \frac{k_9}{2} + \|\boldsymbol{s}_2\|\tilde{D}_t - k_7\boldsymbol{s}_2^{\mathrm{T}}\text{sig}^{\gamma_2}(\boldsymbol{s}_2) + k_{10} \\
&- \frac{1}{c_1}\tilde{D}_r\dot{\tilde{D}}_r - \frac{1}{c_2}\tilde{D}_t\dot{\tilde{D}}_t
\end{aligned} \tag{57}$$

Considering the adaptive laws Eqs. (51)-(52), one has

$$\begin{aligned}
\dot{V}_4 &\le -k_6\boldsymbol{s}_1^{\mathrm{T}}\boldsymbol{s}_1 + \frac{k_9}{2} - k_8\boldsymbol{s}_2^{\mathrm{T}}\boldsymbol{s}_2 + k_{10} + c_3\tilde{D}_r\hat{D}_r + c_4\tilde{D}_t\hat{D}_t \\
&= -k_6\boldsymbol{s}_1^{\mathrm{T}}\boldsymbol{s}_1 + \frac{k_9}{2} - k_8\boldsymbol{s}_2^{\mathrm{T}}\boldsymbol{s}_2 + k_{10} \\
&\quad - c_3\left(D_r - \hat{D}_r\right)^2 + \vartheta_r - c_4\left(D_t - \hat{D}_t\right)^2 + \vartheta_t
\end{aligned} \tag{58}$$

where $\vartheta_r = \frac{c_3^2D_r^2}{4(c_3-1)}$ and $\vartheta_r = \frac{c_4^2D_t^2}{4(c_4-1)}$. Thus, Eq. (58) is further written as:

$$\dot{V}_4 \le -\rho_3V_4 + \vartheta_1 \tag{59}$$

with ϑ_1 and ρ_3 denoting as $\vartheta_1 = \vartheta_r + \vartheta_t + \frac{k_9}{2} + k_{10}$, $\rho_1 = \min\left\{\frac{k_4}{\lambda_{\max}(\boldsymbol{J})}, \frac{k_6}{m}, 2c_1, 2c_2\right\}$.

Thus, it demonstrates that $\boldsymbol{s}_1$, $\boldsymbol{s}_2$, $\tilde{D}_r$, $\tilde{D}_t$ will exponentially coverage to a bounded region with respect to ϑ_1. As a result, there must exist two constants $\bar{D}_r$ and $\bar{D}_r$ satisfying $\bar{D}_r \ge D_r, \bar{D}_r \ge \hat{D}_r, \bar{D}_t \ge D_t, \bar{D}_t \ge \hat{D}_t$. Then, the following LF is presented:

$$V_5 = \frac{1}{2}\boldsymbol{s}_1^{\mathrm{T}}\boldsymbol{J}\boldsymbol{s}_1 + \frac{1}{2}\boldsymbol{s}_2^{\mathrm{T}}m\boldsymbol{s}_2 + \frac{1}{c_1}\left(\bar{D}_r - \hat{D}_r\right)^2 + \frac{1}{c_2}\left(\bar{D}_t - \hat{D}_t\right)^2 \tag{60}$$

Upon utilizing the proposed method, the derivative of V_5 satisfies:

$$\begin{aligned}\dot{V}_5 &= \boldsymbol{s}_1^{\mathrm{T}}\boldsymbol{J}\dot{\boldsymbol{s}}_1+\boldsymbol{s}_2^{\mathrm{T}}m\dot{\boldsymbol{s}}_2-\frac{2}{c_1}\left(\bar{D}_r-\hat{D}_r\right)\dot{\hat{D}}_r-\frac{2}{c_2}\left(\bar{D}_t-\hat{D}_t\right)\dot{\hat{D}}_t\\
&= \boldsymbol{s}_1^{\mathrm{T}}\Bigg[\frac{1}{2}\boldsymbol{J}\left(\dot{\tilde{\boldsymbol{q}}}_v^{\times}+\dot{\tilde{q}}_0\boldsymbol{I}_3\right)\tilde{\boldsymbol{\omega}}+\frac{1}{2}\left(\tilde{\boldsymbol{q}}_v^{\times}+\tilde{q}_0\boldsymbol{I}_3\right)\\
&\quad\times\left(-\boldsymbol{C}_r\tilde{\boldsymbol{\omega}}-\boldsymbol{n}_r+\boldsymbol{\varepsilon}_r+\boldsymbol{\tau}_d\right)+k_1\dot{\tilde{\boldsymbol{q}}}_v\\
&\quad+k_2\boldsymbol{J}\left(1+\tanh^{\mathrm{T}}\left(\tilde{\boldsymbol{q}}_v\right)\tanh\left(\tilde{\boldsymbol{q}}_v\right)\right)\dot{\tilde{\boldsymbol{q}}}_v\Bigg]\\
&\quad+\boldsymbol{s}_2^{\mathrm{T}}\Big[-m\boldsymbol{C}_t\tilde{\boldsymbol{v}}-m\boldsymbol{n}_t+\boldsymbol{\varepsilon}_t+\boldsymbol{f}_d-m\boldsymbol{C}_t\dot{\tilde{\boldsymbol{r}}}+k_3\dot{\tilde{\boldsymbol{r}}}\\
&\quad-m\dot{\boldsymbol{C}}_t\tilde{\boldsymbol{r}}+k_4\left(1+\tanh^{\mathrm{T}}\left(\tilde{\boldsymbol{r}}\right)\tanh\left(\tilde{\boldsymbol{r}}\right)\right)\dot{\tilde{\boldsymbol{r}}}\Big]\\
&\quad-\frac{2}{c_1}\left(\bar{D}_r-\hat{D}_r\right)\dot{\hat{D}}_r-\frac{2}{c_2}\left(\bar{D}_t-\hat{D}_t\right)\dot{\hat{D}}_t\\
&= \boldsymbol{s}_1^{\mathrm{T}}\left(\frac{1}{2}\left(\tilde{\boldsymbol{q}}_{\mathrm{v}}^{\times}+\tilde{q}_0\boldsymbol{I}_3\right)\boldsymbol{\tau}_d-k_5\mathrm{sig}^{\gamma_1}\left(\boldsymbol{s}_1\right)-k_6\boldsymbol{s}_1\right.\\
&\quad\left.-\frac{\hat{D}_r\boldsymbol{s}_1}{2\left\|\boldsymbol{s}_1\right\|+\varepsilon_1}\right)+\boldsymbol{s}_2^{\mathrm{T}}\left(\boldsymbol{f}_d-k_7\mathrm{sig}^{\gamma_2}\left(\boldsymbol{s}_2\right)\right.\\
&\quad\left.-k_8\boldsymbol{s}_2-\frac{\hat{D}_t\boldsymbol{s}_2}{\left\|\boldsymbol{s}_2\right\|+\varepsilon_2}\right)-\frac{2}{c_1}\left(\bar{D}_r-\hat{D}_r\right)\dot{\hat{D}}_r\\
&\quad-\frac{2}{c_2}\left(\bar{D}_t-\hat{D}_t\right)\dot{\hat{D}}_t\\
&\leq \frac{\left\|\boldsymbol{s}_1\right\|}{2}\tilde{D}_t+\left\|\boldsymbol{s}_2\right\|\tilde{D}_t-k_5\boldsymbol{s}_1^{\mathrm{T}}\mathrm{sig}^{\gamma_1}\left(\boldsymbol{s}_1\right)+\frac{k_9}{2}\\
&\quad-k_7\boldsymbol{s}_2^{\mathrm{T}}\mathrm{sig}^{\gamma_2}\left(\boldsymbol{s}_2\right)+k_{10}-\frac{2}{c_1}\left(\bar{D}_r-\hat{D}_r\right)\dot{\hat{D}}_r\\
&\quad-\frac{2}{c_2}\left(\bar{D}_t-\hat{D}_t\right)\dot{\hat{D}}_t \qquad (61)\end{aligned}$$

Inserting the adaptive laws defined in Eqs. (51)-(52) into Eq. (61) yields:

$$\begin{aligned}\dot{V}_5 &\leq \frac{\left\|\boldsymbol{s}_1\right\|}{2}\left(\bar{D}_r-\hat{D}_r\right)+\left\|\boldsymbol{s}_2\right\|\left(\bar{D}_r-\hat{D}_r\right)\\
&\quad-k_5\boldsymbol{s}_1^{\mathrm{T}}\mathrm{sig}^{\gamma_1}\left(\boldsymbol{s}_1\right)-k_7\boldsymbol{s}_2^{\mathrm{T}}\mathrm{sig}^{\gamma_2}\left(\boldsymbol{s}_2\right)+\frac{k_9}{2}\\
&\quad+k_{10}-2c_3\left(\bar{D}_r-\hat{D}_r\right)\hat{D}_r-2c_4\left(\bar{D}_t-\hat{D}_t\right)\hat{D}_t\\
&\leq -\rho_4\min\left(V_5^{\frac{1}{2}},V_5^{\frac{\gamma_1+1}{2}},V_5^{\frac{\gamma_2+1}{2}}\right)+\vartheta_2 \qquad (62)\end{aligned}$$

where $\rho_4 = \min\left\{\frac{2^{\frac{\gamma_1+1}{2}}k_5}{\lambda_2^{\frac{\gamma_1+1}{2}}},\frac{2^{\frac{\gamma_2+1}{2}}k_7}{m^{\frac{\gamma_2+1}{2}}},\frac{\sqrt{c_1}\left\|\boldsymbol{s}_1\right\|}{2},\sqrt{c_1}\left\|\boldsymbol{s}_2\right\|\right\}$, $\vartheta_2=\frac{c_3\tilde{D}_r^2+c_4\tilde{D}_t^2}{2}+\frac{k_9}{2}+k_{10}$. Thus, the $\boldsymbol{s}_1$ and $\boldsymbol{s}_2$ will converge to the region Δ_2 in finite time, where $\Delta_2$is a positive constant. Based on this fact, the following equation can be obtained:

$$\dot{\tilde{q}}_{vi}+k_1\tilde{q}_{vi}+k_2\tanh\left(\tilde{q}_{vi}\right)\leq\Delta_2 \qquad (63)$$

$$\dot{\tilde{r}}_i+k_3\tilde{r}_i+k_4\tanh\left(\tilde{r}_i\right)\leq\Delta_2 \qquad (64)$$

The following LF is constructed to illustrate the stability of the tracking errors:

$$V_6=\frac{1}{2}\tilde{q}_{vi}^2+\frac{1}{2}r_i^2 \qquad (65)$$

According to Eqs. (63)-(64), the derivative of V_6 satisfies

$$\begin{aligned}\dot{V}_6 &= \tilde{q}_{vi}\dot{\tilde{q}}_{vi}+\tilde{r}_i\dot{\tilde{r}}_i\\
&\leq \tilde{q}_{vi}\left(\Delta_2-k_1\tilde{q}_{vi}-k_2\tanh\left(\tilde{q}_{vi}\right)\right)\\
&\quad+\tilde{r}\left(\Delta_2-k_3\tilde{r}_i-k_4\tanh\left(\tilde{r}_i\right)\right)\\
&\leq -k_1\left|\tilde{q}_{vi}\right|-k_3\left|\tilde{r}_i\right|+\left(k_1+k_3\right)\kappa+\frac{\Delta^2}{4}\\
&\leq -\sqrt{2}\min\left(k_3+k_1\right)V_6^{\frac{1}{2}}+\left(k_1+k_3\right)\kappa+\frac{\Delta^2}{4} \qquad (66)\end{aligned}$$

Thus, tracking errors $\tilde{q}_{vi}$ and $\tilde{r}_i$ will converge to a small region containing zero in finite time.

Thus, Theorem 2 has been proven.

IV. SIMULATION RESULTS

To show that the achievability of the control objective under the developed control algorithm, the rendezvous maneuver scenario is adopted in this section, where a pursuer spacecraft is forced to rendezvous with the target spacecraft in an elliptical orbit. Detailed information about the orbit and these two spacecrafts is presented in the following table.

TABLE 1. Orbit and spacecraft information [30].

Parameter	Value	Unit
Gravitational constant, μ	6.371	km
Eccentricity, e	0.3	—
Radius of the Earth, R_E	6371	km
Perigee altitude, r_{pa}	400	km
Initial true anomaly, $v(0)$	10	degrees
Inertial matrix, $\boldsymbol{J}$	diag(20,20,15)	kg·m^2
Inertial matrix, $\boldsymbol{J}_t$	diag(26,16,21)	kg·m^2
Mass, m	90	kg
Mass, m_t	150	kg

The target spacecraft is supposed to service with the following position:

$$\boldsymbol{r}_t=\left[r_t,0,0\right]^{\mathrm{T}},\quad r_t=\frac{a\left(1-e^2\right)}{1+e\cos v} \qquad (67)$$

where $a = R_E+\frac{r_{pa}}{1-e}$ denotes the semimajor axis, v is expressed as:

$$\dot{v}=\frac{n\left(1+e\cos v\right)^2}{\left(1-e^2\right)^{\frac{3}{2}}},\quad \ddot{v}=\frac{2n^2e\left(1+e\cos v\right)^3\sin v}{\left(1-e^2\right)^3} \qquad (68)$$

where $n=\sqrt{u/a^3}$. For the pursuer spacecraft, its rendezvous position is expected as $\boldsymbol{\delta}_t=[0,5,0]^{\mathrm{T}}$ in the target's body coordinate frame. The angular velocity of the target and the external disturbances are given as:

$$\boldsymbol{\tau}_d=0.002\times\left(1+\cos\left(\frac{\pi}{150}t\right)+\sin\left(\frac{\pi}{150}t\right)\right)[1;1;1]^{\mathrm{T}}\ \mathrm{N\cdot m}$$

$$\boldsymbol{f}_d=0.001\times\left(1+\cos\left(\frac{\pi}{150}t\right)+\sin\left(\frac{\pi}{150}t\right)\right)[1;1;1]^{\mathrm{T}}\ \mathrm{N\cdot m}$$

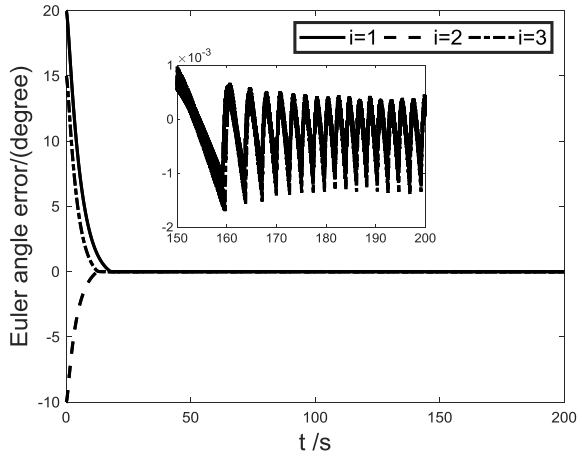

FIGURE 1. Euler angle.

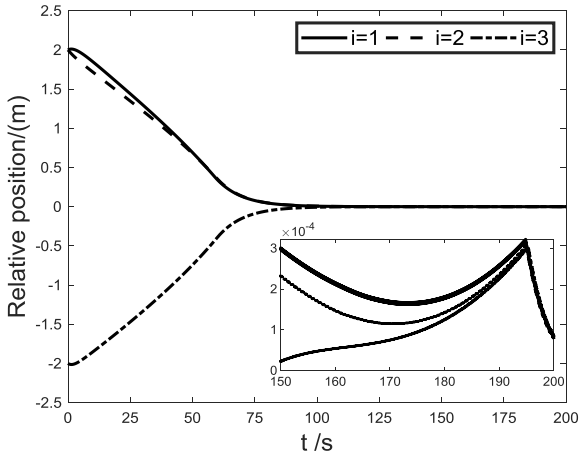

FIGURE 3. Relative position.

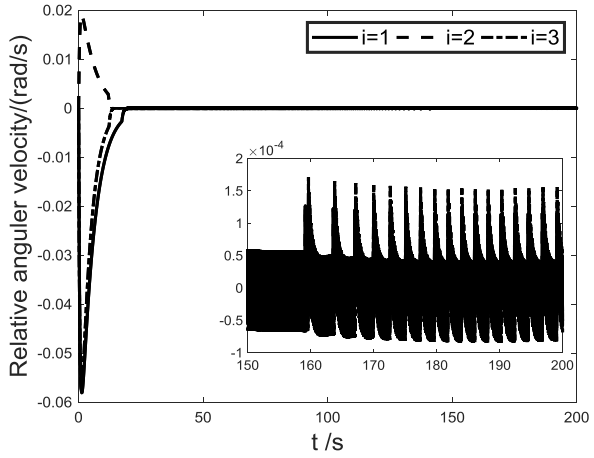

FIGURE 2. Regular angular velocity.

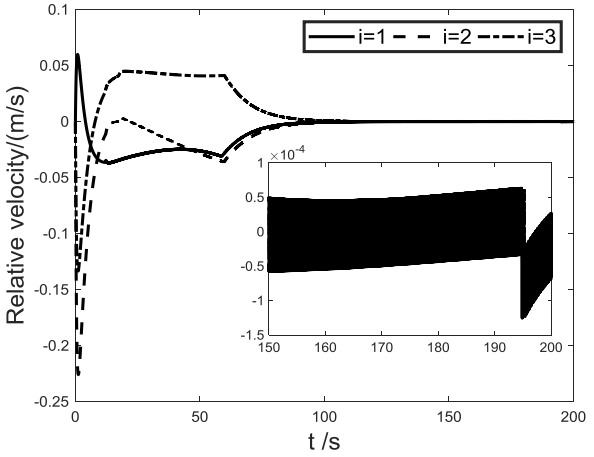

FIGURE 4. Relative velocity.

According to the ingenious initial parameters in [34], the initial states are set as: the initial Euler angle error is $\Theta(0) = [19.9984 - 9.9987\ 15.0050]^{\mathrm{T}}$ deg, $\tilde{\boldsymbol{\omega}} = [000]^{\mathrm{T}}$, $\tilde{\boldsymbol{r}}(0) = [2,2,-2]^{\mathrm{T}}$ and $\tilde{\boldsymbol{v}}(0) = [000]^{\mathrm{T}}$.

Inspired by the algorithms in [33], simulations are conducted via MATLAB such that the effectiveness of the presented methods can be validated. There are eight parameters in the first controller and sixteen parameters in the second controller. For the first controller, the settling time is mainly decided by $k_1, k_2, k_3, k_4\ k_5$ and k_6. More specifically, the settling time will increase as k_1 and k_2 increase while it will decrease as k_4 and k_6 increase. However, increasing k_3 and k_5 will aggravate chattering phenomenon. The relative attitude and position heavily depend on k_4 and k_6. Nevertheless, improving the control accuracy will need much more control input.

Considering the external disturbance, c_1 and c_2 must be selected properly. For the second controller, there are another four parameters: k_7, k_8, $c_3$and c_4. These four parameters are added to accommodate the influence of the disturbance and ensure upper bounds for the estimates of the adaptive parameters.

A. SIMULATION RESULTS OF THE BASIC CONTROLLER

In the basic controller, the design parameters are selected as: $k_1 = 2$, $k_2 = 0.1$, $k_3 = 0.05$, $k_4 = 4$, $k_5 = 0.5$, $k_6 = 5$, $c_1 = 0.01$, $c_2 = 0.01$, $\hat{D}_r(0) = 0$, $\hat{D}_t(0) = 0$. The simulation results are presented in Figs. 1-8. Fig. 1 and Fig. 2 depict he Euler angle error and relative angular velocity, which implies that the attitude control will be completed within 20s under the basic controller. Figs. 3-4 present the orbit control results, where the relative position and velocity are depicted. Figs. 5-8 are the control torques $\boldsymbol{\tau}, \boldsymbol{f}$ and estimated parameters $\hat{D}_r, \hat{D}_r$, respectively. From the foregoing results, one can find that the rendezvous maneuver will be achieved in finite time.

B. SIMULATION RESULTS OF THE CHATTERING-FREE CONTROLLER

Observing the presented results in Figs 5-6, it is concluded that chattering problem exists in the basic controller.

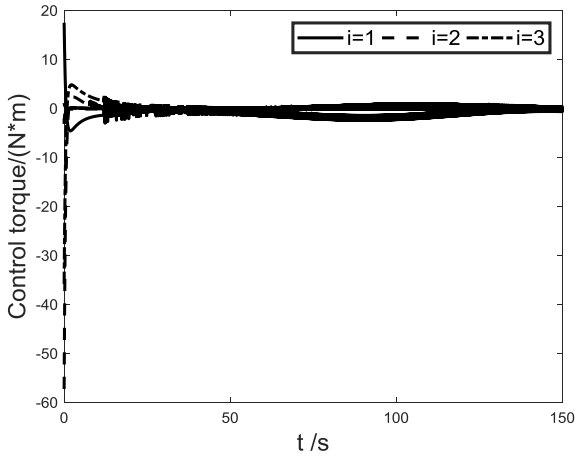

FIGURE 5. The control torque τ.

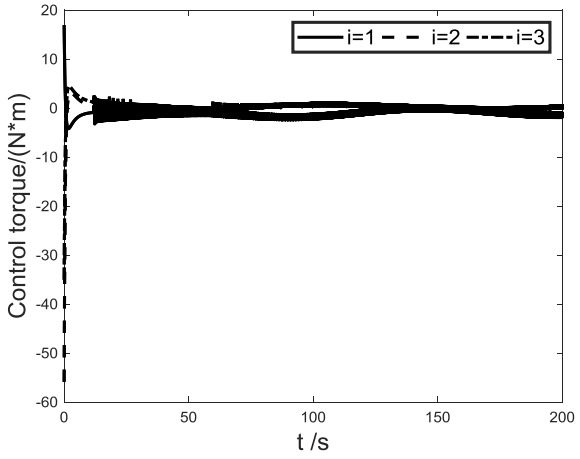

FIGURE 6. The control torque f.

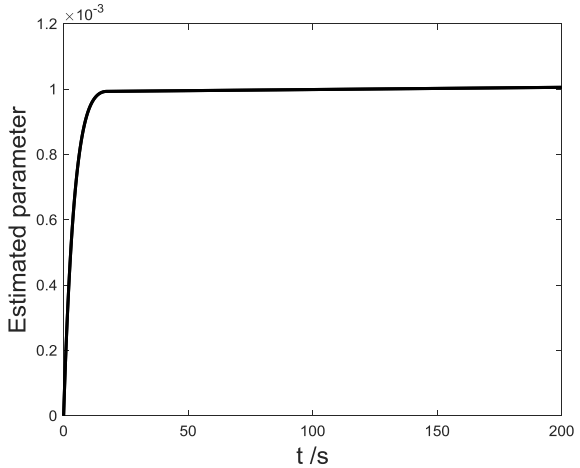

FIGURE 7. The estimated parameter $\hat{D}_r$.

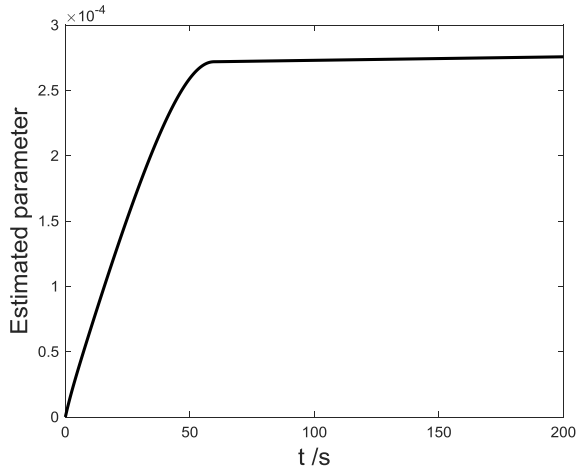

FIGURE 8. The estimated parameter $\hat{D}_t$.

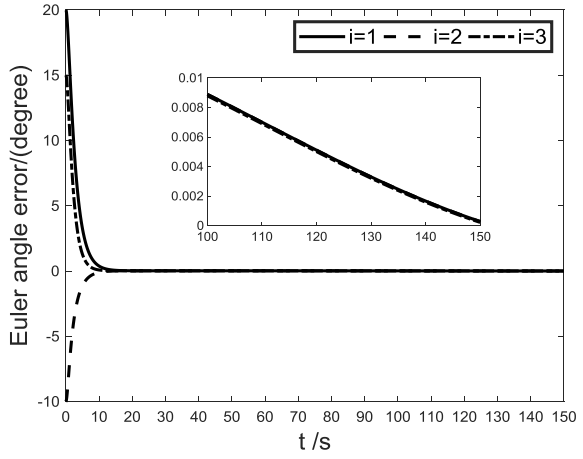

FIGURE 9. Euler angle.

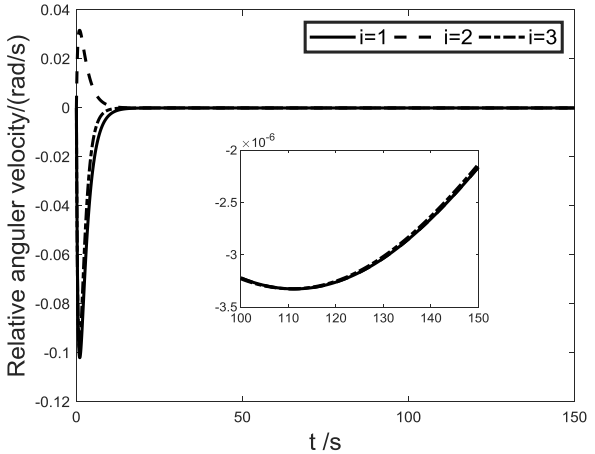

FIGURE 10. Regular angular velocity.

To overcome this defect, the chattering-free controller will be adopted in this subsection. The control parameters are given as: $k_1 = 2, k_2 = 2, k_3 = 1.1, k_4 = 0.1, k_5 = 0.05, k_6 = 4, k_7 = 0.5, k_8 = 5, k_9 = 0.001, k_{10} = 0.001, c_1 = 0.01, c_2 = 0.01, c_3 = 0.01, c_4 = 0.01, \gamma_1 = 1, \gamma_2 = 1, \hat{D}_r(0) = 0, \hat{D}_t(0) = 0$. The corresponding simulation results are shown in Figs. 9-16. Fig. 9 and Fig. 10 depict the Euler angle error and relative angular velocity, which implies

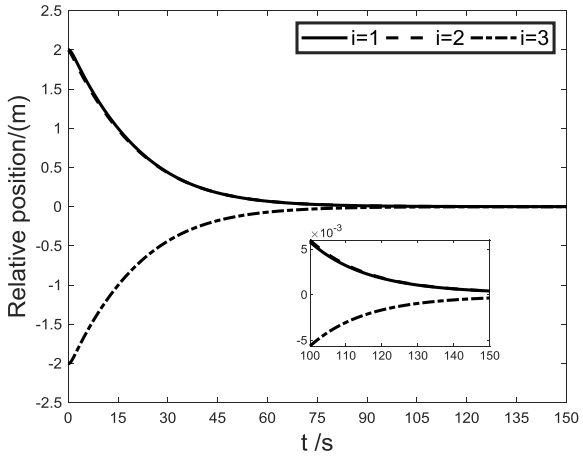

FIGURE 11. Relative position.

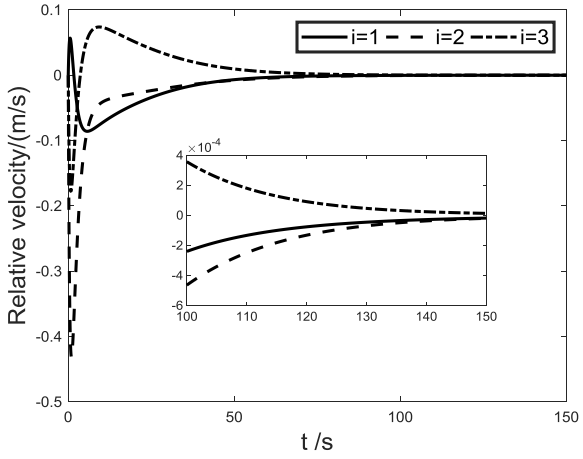

FIGURE 12. Relative velocity.

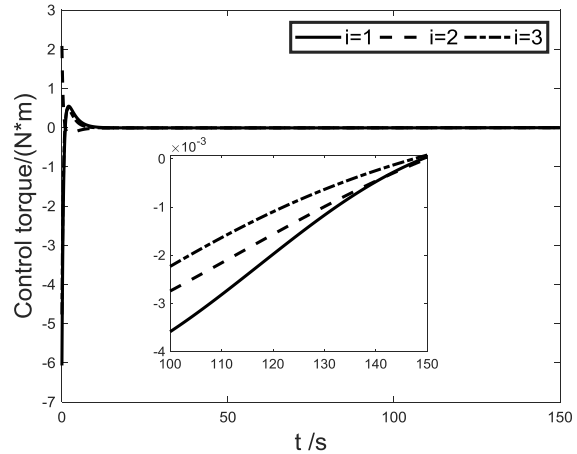

FIGURE 13. The control torque τ.

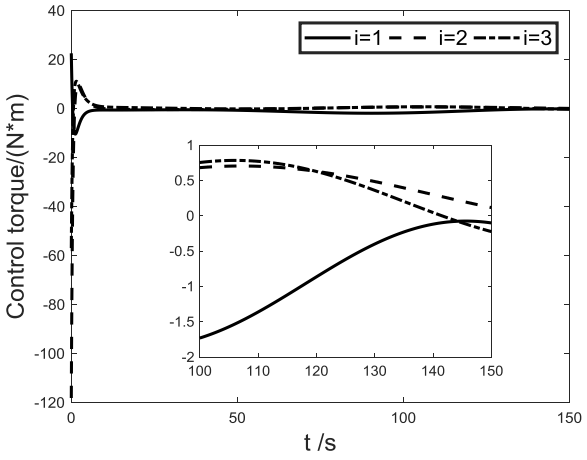

FIGURE 14. The control torque f.

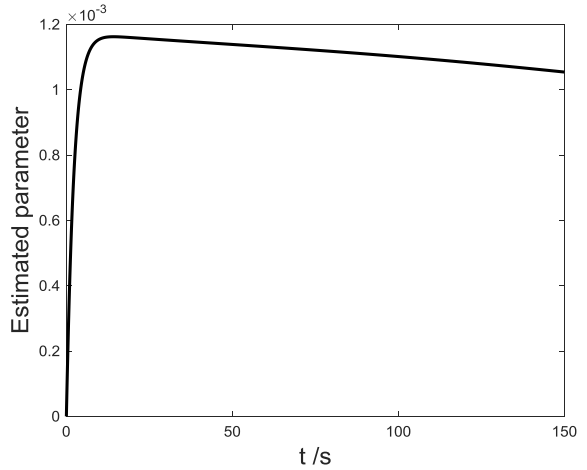

FIGURE 15. The estimated parameter $\hat{D}_f$.

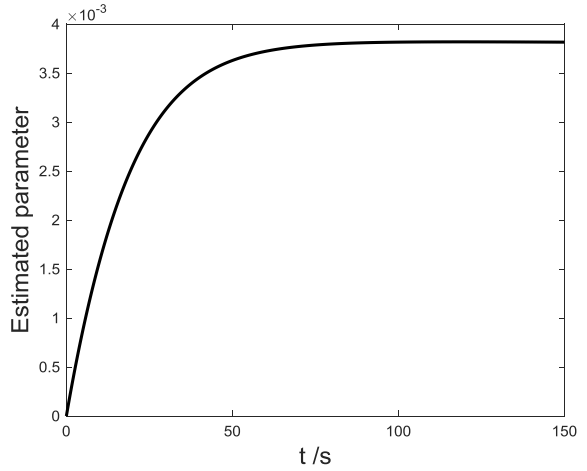

FIGURE 16. The estimated parameter $\hat{D}_t$.

that the attitude control will be completed within 10s under the basic controller. Comparing with the basic controller, the chattering free control scheme possesses faster convergence rate. The relative position, relative velocity and control torques are presented in Figs. 11-14. Obviously, the chattering phenomenon will not exist in the second controller, thus effectively prolonging the service life of the spacecraft. The estimated parameters are depicted in Figs. 15-16,

which imply that the upper bound of the disturbance will be well estimated.

V. CONCLUSION

The robust rendezvous maneuver control problem for spacecraft was solved via finite-time theorem and sliding mode technology. The proposed SMS possesses finite-time convergence and the singularity problem is tackled via the hyperbolic tangent function. Additionally, the chattering phenomenon is eliminated even when the sliding mode method is used. The effectiveness of the proposed methods is illustrated by theoretical analysis and numerical simulations.

REFERENCES

[1] L.-G. Gong, Q. Wang, and C.-Y. Dong, "Spacecraft output feedback attitude control based on extended state observer and adaptive dynamic programming," *J. Franklin Inst.*, vol. 356, no. 10, pp. 4971–5000, Jul. 2019.
[2] C. Wang, L. Guo, C. Wen, Q. Hu, and J. Qiao, "Event-triggered adaptive attitude tracking control for spacecraft with unknown actuator faults," *IEEE Trans. Ind. Electron.*, vol. 67, no. 3, pp. 2241–2250, Mar. 2020.
[3] H. Gui and G. Vukovich, "Adaptive fault-tolerant spacecraft attitude control using a novel integral terminal sliding mode," *Int. J. Robust Nonlinear Control*, vol. 27, no. 16, pp. 3174–3196, Nov. 2017.
[4] T. Chen and G. Chen, "Distributed adaptive tracking control of multiple flexible spacecraft under various actuator and measurement limitations," *Nonlinear Dyn.*, vol. 91, no. 3, pp. 1571–1586, Feb. 2018.
[5] L. Zhao, J. Yu, and P. Shi, "Command filtered backstepping-based attitude containment control for spacecraft formation," *IEEE Trans. Syst., Man, Cybern., Syst.*, early access, Feb. 22, 2019, doi: 10.1109/TSMC.2019.2896614.
[6] F. Wang, M. Hou, X. Cao, and G. Duan, "Event-triggered backstepping control for attitude stabilization of spacecraft," *J. Franklin Inst.*, vol. 356, no. 16, pp. 9474–9501, Nov. 2019.
[7] Z. Chen, Q. Chen, X. He, and M. Sun, "Adaptive backstepping control design for uncertain rigid spacecraft with both input and output constraints," *IEEE Access*, vol. 6, pp. 60776–60789, 2018.
[8] Y. Wang, S. Tang, X. Wang, C. Liu, and J. Guo, "Fuzzy-logic-based fixed-time geometric backstepping control on SO(3) for spacecraft attitude tracking," *IEEE Trans. Aerosp. Electron. Syst.*, vol. 55, no. 6, pp. 2938–2950, Dec. 2019.
[9] N. Zhou, R. Chen, Y. Xia, J. Huang, and G. Wen, "Neural network-based reconfiguration control for spacecraft formation in obstacle environments," *Int. J. Robust Nonlinear Control*, vol. 28, no. 6, pp. 2442–2456, Apr. 2018.
[10] R. Sun, J. Wang, D. Zhang, and X. Shao, "Neural network-based sliding mode control for atmospheric-actuated spacecraft formation using switching strategy," *Adv. Space Res.*, vol. 61, no. 3, pp. 914–926, Feb. 2018.
[11] L. Zhao and Y. Jia, "Neural network-based distributed adaptive attitude synchronization control of spacecraft formation under modified fast terminal sliding mode," *Neurocomputing*, vol. 171, pp. 230–241, Jan. 2016.
[12] X. Cao, P. Shi, Z. Li, and M. Liu, "Neural-network-based adaptive backstepping control with application to spacecraft attitude regulation," *IEEE Trans. Neural Netw. Learn. Syst.*, vol. 29, no. 9, pp. 4303–4313, Sep. 2018.
[13] Y. Guo, B. Huang, S.-M. Song, A.-J. Li, and C.-Q. Wang, "Robust saturated finite-time attitude control for spacecraft using integral sliding mode," *J. Guid., Control, Dyn.*, vol. 42, no. 2, pp. 440–446, Feb. 2019.
[14] Y. Guo, B. Huang, J.-H. Guo, A.-J. Li, and C.-Q. Wang, "Velocity-free sliding mode control for spacecraft with input saturation," *Acta Astronautica*, vol. 154, pp. 1–8, Jan. 2019.
[15] B. Huang, A.-J. Li, Y. Guo, and C.-Q. Wang, "Rotation matrix based finite-time attitude synchronization control for spacecraft with external disturbances," *ISA Trans.*, vol. 85, pp. 141–150, Feb. 2019.
[16] B. Huang, A.-J. Li, Y. Guo, and C.-Q. Wang, "Fixed-time attitude tracking control for spacecraft without unwinding," *Acta Astronautica*, vol. 151, pp. 818–827, Oct. 2018.
[17] L. Sun, W. Huo, and Z. Jiao, "Adaptive backstepping control of spacecraft rendezvous and proximity operations with input saturation and full-state constraint," *IEEE Trans. Ind. Electron.*, vol. 64, no. 1, pp. 480–492, Jan. 2017.
[18] K. Li and H. Ji, "Inverse optimal adaptive backstepping control for spacecraft rendezvous on elliptical orbits," *Int. J. Control*, vol. 91, no. 10, pp. 2303–2313, Oct. 2018.
[19] K. Xia and W. Huo, "Robust adaptive backstepping neural networks control for spacecraft rendezvous and docking with input saturation," *ISA Trans.*, vol. 62, pp. 249–257, May 2016.
[20] K. Zhang and G. R. Duan, "Robust H_∞ dynamic output feedback control for spacecraft rendezvous with poles and input constraint," *Int. J. Syst. Sci.*, vol. 48, no. 5, pp. 1022–1034, 2017.
[21] Q. Li, B. Zhang, J. Yuan, and H. Wang, "Potential function based robust safety control for spacecraft rendezvous and proximity operations under path constraint," *Adv. Space Res.*, vol. 62, no. 9, pp. 2586–2598, Nov. 2018.
[22] Q. Li, J. Yuan, B. Zhang, and H. Wang, "Artificial potential field based robust adaptive control for spacecraft rendezvous and docking under motion constraint," *ISA Trans.*, vol. 95, pp. 173–184, Dec. 2019.
[23] B. Jiang, Q. Hu, and M. I. Friswell, "Fixed-time rendezvous control of spacecraft with a tumbling target under loss of actuator effectiveness," *IEEE Trans. Aerosp. Electron. Syst.*, vol. 52, no. 4, pp. 1576–1586, Aug. 2016.
[24] S. He, D. Lin, and J. Wang, "Autonomous spacecraft rendezvous with finite time convergence," *J. Franklin Inst.*, vol. 352, no. 11, pp. 4962–4979, Nov. 2015.
[25] Y. Wang and H. Ji, "Integrated relative position and attitude control for spacecraft rendezvous with ISS and finite-time convergence," *Aerosp. Sci. Technol.*, vol. 85, pp. 234–245, Feb. 2019.
[26] G.-Q. Wu and S.-M. Song, "Antisaturation attitude and orbit-coupled control for spacecraft final safe approach based on fast nonsingular terminal sliding mode," *J. Aerosp. Eng.*, vol. 32, no. 2, Mar. 2019, Art. no. 04019002.
[27] G.-Q. Wu, S.-M. Song, and J.-G. Sun, "Finite-time antisaturation control for spacecraft rendezvous and docking with safe constraint," *Proc. Inst. Mech. Eng. G, J. Aerosp. Eng.*, vol. 233, no. 6, pp. 2170–2184, May 2019.
[28] M. J. Sidi, *Spacecraft Dynamics and Control: A Practical Engineering Approach*. Cambridge, U.K.: Cambridge Univ. Press, 1997.
[29] L. Zhang, B. Huang, Y. Liao, and B. Wang, "Finite-time trajectory tracking control for uncertain underactuated marine surface vessels," *IEEE Access*, vol. 7, pp. 102321–102330, 2019.
[30] K. Xia and S.-Y. Park, "Adaptive control for spacecraft rendezvous subject to time-varying inertial parameters and actuator faults," *J. Aerosp. Eng.*, vol. 32, no. 5, Sep. 2019, Art. no. 04019063.
[31] S. Di Cairano, H. Park, and I. Kolmanovsky, "Model predictive control approach for guidance of spacecraft rendezvous and proximity maneuvering," *Int. J. Robust Nonlinear Control*, vol. 22, no. 12, pp. 1398–1427, Aug. 2012.
[32] P. Singla, K. Subbarao, and J. L. Junkins, "Adaptive output feedback control for spacecraft rendezvous and docking under measurement uncertainty," *J. Guid., Control, Dyn.*, vol. 29, no. 4, pp. 892–902, Jul. 2006.
[33] X. Wu, W. Bai, Y. Xie, X. Sun, C. Deng, and H. Cui, "A hybrid algorithm of particle swarm optimization, metropolis criterion and RTS smoother for path planning of UAVs," *Appl. Soft Comput.*, vol. 73, no. 12, pp. 735–747, Dec. 2018.
[34] X. Sun, X. Wu, W. Chen, Y. Hao, K. A. Mantey, and H. Zhao, "Dual quaternion based dynamics modeling for electromagnetic collocated satellites of diffraction imaging on geostationary orbit," *Acta Astronautica*, vol. 166, pp. 52–58, Jan. 2020.
[35] Y.-H. Wu, F. Han, S.-J. Zhang, B. Hua, and Z.-M. Chen, "Attitude agile maneuvering control for spacecraft equipped with hybrid actuators," *J. Guid., Control, Dyn.*, vol. 41, no. 3, pp. 809–812, Mar. 2018.

ZHEN SHI received the B.S. degree in aerospace engineering and the M.S. degree in control engineering from the Institute of Harbin Shipbuilding Engineering, in 1982 and 1986, respectively, and the Ph.D. degree in control engineering from Harbin Engineering University, in 2001. Since 2001, he has been a Professor with Harbin Engineering University. His research interests include the guidance and control technology for aircraft, the control theory and its application, and the strap-down inertial navigation technology.

CHENGCHEN DENG received the bachelor's degree from the Nanjing University of Science and Technology, in 2007, and the master's degree from Sichuan University, in 2013. He is currently pursuing the Ph.D. degree with Harbin Engineering University. His research interests include robust control, nonlinear control for spacecraft, formation tracking control for satellite formation, fault-tolerant control, sliding mode control, and intelligent control.

SAI ZHANG was born in Anhui, China, in 1998. He is currently pursuing the bachelor's degree in aircraft design and engineering with Harbin Engineering University. His research interests include spacecraft dynamics, fault-tolerant control, and sliding mode control.

YAEN XIE, photograph and biography not available at the time of publication.

HONGTAO CUI received the bachelor's and master's degrees from Heilongjiang University, in 2013 and 2016, respectively. He is currently pursuing the Ph.D. degree with Harbin Engineering University. His research interests include spacecraft dynamics modeling and control and multibody dynamics modeling and control.

YONG HAO received the bachelor's degree in automation and the master's and Ph.D. degrees from Harbin Engineering University, in 2003, 2009, and 2016, respectively. He is currently a Lecturer at the College of Automation, Harbin Engineering University. His research interests include planning the attitude of agile imaging satellite, formation attitude control, and sliding mode control.